Active figure control effects on mounting strategy for x-ray optics

Jeffery J. Kolodziejczak[*a], Carolyn Atkins[b], Jacqueline M. Roche[a], Stephen L. O'Dell[a], Brian D. Ramsey[a], Ronald F. Elsner[a], Martin C. Weisskopf[a], and Mikhail V. Gubarev[a].
[a] NASA Marshall Space Flight Center, Space Science Office, MSFC/ZP12, Huntsville, AL 35812 [b] University of Alabama in Huntsville, Huntsville, AL 35899

ABSTRACT

As part of ongoing development efforts at MSFC, we have begun to investigate mounting strategies for highly nested x-ray optics in both full-shell and segmented configurations. The analytical infrastructure for this effort also lends itself to investigation of active strategies. We expect that a consequence of active figure control on relatively thin substrates is that errors are propagated to the edges, where they might affect the effective precision of the mounting points. Based upon modeling, we describe parametrically, the conditions under which active mounts are preferred over fixed ones, and the effect of active figure corrections on the required number, locations, and kinematic characteristics of mounting points.

Keywords: x-ray optics, active optics, optomechanical modeling, x-ray telescopes.

1. INTRODUCTION

At MSFC, we are involved in several technology development efforts for higher resolution, larger area, and lighter weight x-ray optics to support future replacement of the 15-year-old *Chandra X-ray Observatory,*[1-4] with the next mission to attain sub-arcsecond x-ray imaging. All of these technologies[5-15] share the need to be mounted, assembled, and aligned into modular units for testing or for flight. Because in our recent experience with moderate-resolution optics[16-20] we have found that without considerable development effort, it is difficult to prevent structure induced errors from contributing significantly, i.e. factors of 1.4-2, to the overall resolution, we have identified a requirement to develop the capability to assess the impact of mounting designs and processes on performance.[21,22] This development is in very early stages for active optics, so results thus far, are relatively simplistic, naïve, and incomplete. Nevertheless, we expect that including active optics mounting strategies in our repertoire will help to drive our understanding of technical challenges and capabilities to overcome them to a higher level in the future.

In this paper we will discuss challenges related to aligning and mounting ~1 arcsec x-ray optics for space applications and describe the system-level approach we are taking to begin to understand the drivers in going from <1 arcsec thin optical segments to <1 arcsec highly–nested module assemblies and telescopes. Because many groups are working on many technologies for producing precision shells or segments, we have developed a rather general and flexible set of techniques. In this paper we will focus on the specific implications for active figure control and specifically bimorph-driven adjustable optics. It would seem apparent that an active mounting scheme would make moot the significance of any differences between mounting strategy for active and passive optics. However the cost and complexity of such a scheme may delay its implementation beyond the next high- resolution x-ray mission. Herein, we will consider only passive strategies.

1.1 Objectives

General considerations for mounting a segment

Optomechanical structures are designed to perform a very specific task – to hold an optical surface in place to attain the required performance over the required range of operating conditions within a set of prerequisite design constraints. The ongoing efforts among several groups to develop high precision optical elements for highly nested systems will eventually require mounting schemes in which the supporting structure mass and volume per square centimeter of effective area must be far smaller than has ever been achieved for <1 arcsec x-ray optics. *Chandra* needed approximately 400 kg of support structure to hold sub-arc-second tolerances on the metric ton of optics with a clear aperture area of

[*] kolodz@nasa.gov;

1145 cm^2. For a future straw man concept such as *SMART-X*,[23] the optics are roughly one-half, with support structure of three halves the mass of *Chandra's* mirrors and support structure, and with 30 times the area. Thus we are driving to improve the mass efficiency for the support structures by at least a factor of 20 from around 1/3 kg/cm^2 to <17 g/cm^2. The nesting will leave ~1mm between radially adjacent segments compared with *Chandra's* 10 cm, making attachment points anywhere except the edges of the glass problematic.

We note the alignment and assembly specifications for Chandra described in ref. 24 segregated into alignment constraints on individual segment pairs and confocality requirements among pairs after assembly into modules and then the final telescope system. For alignment these were 0.1 arcsec for the relative tilt, 0.005 mm for decenter and 5 mm for despacing. For assembly requirements were 0.025 mm for axial parfocalization and 0.0025 mm for radial parfocalization. Given adequately figured optics, the mounting requirements are to place the optics at the prescribed locations within these tolerances while not distorting the as-mounted figure beyond required levels. In summary, a support structure affects the telescope performance in 2 ways: 1) the tolerances on the average position and orientation of each optic and 2) the distortions in the figure of a given optic introduced by any applied mounting forces.

Specific considerations for adjustable segments

Adjustable optics impacts the strategy for support structure design in a number of ways. Mounting points constrain the ability of bimorphs to correct initial figure errors. Mounting points also introduce additional distortions for the bimorphs to correct. The bimorph corrections are ineffective at the edges, where the mounting points are likely to be, thereby reducing the tolerances of the mounting points themselves. But the bimorph corrections can also ease tolerances by enabling figure adjustments to account for as-built position and orientation errors. Table 1 summarizes our initial perception of the advantages and disadvantages of figure adjustability from the standpoint of mounting structure design.

Table 1. Perceived advantages and disadvantages of adjustable optics from the mounting standpoint.

Effect on:	Advantages	Disadvantages
Tolerances on the average position and orientation of each optic	• Figure adjustable to account for position and orientation errors	• Inability to correct figure errors near edges may require compensation in the form of tighter mounting tolerances
Distortions in the figure of a given optic introduced by any applied mounting forces	• Able to apply corrections to compensate for induced distortions	• Bimorph effectiveness is reduced near mounting points, reducing ability to correct for initial figure error and distortions

We plan to improve our understanding of the importance of these potential benefits and drawbacks through the analytical process described below. The key questions to be addressed are:

- What kinds of distortions are uncorrectable by bimorphs?
- How are uncorrectable distortions minimized?
  - Which design parameters?
  - Which process techniques?
  - In what sequence are processes performed?
- To what degree can figure be adjusted to account for mount-induced position and orientation errors?

Our overall goal is to develop testable high-performance mounting options for specific x-ray optics technologies, which would be applicable to a fully developed manufacturing process. This applies for the specific case of adjustable optics as well, but we will first work to identify the important distinctions from immutable segmented optics.

1.2 System Level Approach

Alignment and assembly are steps in a manufacturing process to produce performance-optimized large-area actively controlled x-ray optics modules. The complete process is likely to involve a very large trade space of technological methods, design parameters, and process sequences. Figure 1 is an illustration of a segment of the process, annotated with potential influence of each individual step on resulting optical performance. We anticipate benefit from the early

development of high-fidelity simulations as a tool to illuminate the tall poles in the error budget, guide the choices toward performance optimization, and enable strategic comparisons by providing an integrated end-to-end measure of the entire process.[25,26] Our *Chandra* experience has shown that multiple independent performance predictions are needed to inject sufficient discourse into the development process to have confidence that test results will satisfy requirements,[27,28,29] so we approach the problem by starting to develop a flexible set of tools, which are specific to the mounting and alignment problem and independent of other likely methods.

As the technology progresses, we plan to be guided by test results on prototypes and engineering models, but for now our end-to-end performance predictions will rely on simulations to begin to answer key questions. We begin by developing deflection models based on plate/shallow shell theory and validate against FEM, and then proceed to develop and apply boundary conditions as appropriate to address the questions in terms of figure distortions before finally, computing an influence function basis for response to bimorph actuation. We then generate large samples of initial figure error maps, and fit this basis to initial figure plus distortions to determine the final figure that minimizes RMS axial slope errors or RMS 2-reflection ray errors. We currently implement ordinary least squares fitting, since the goal is not to provide a precise set of actuator voltages, but merely to evaluate mounting and alignment options. We do implement a check on fit results to ensure no run-away voltages. By compare results from configuration alternatives we will begin to narrow the range of alternatives as illustrated in the more detailed discussion in subsequent sections.

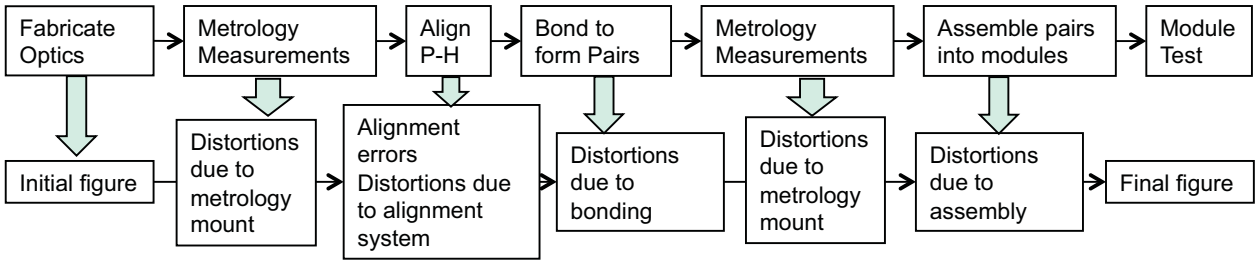

Figure 1. Illustration of a simplified process flow segment between optic fabrication and module test. Each step has the potential to impact the final figure in one or more ways. Generally, as precision requirements tighten, the fraction of these steps that actually do impact performance increases.

2. METHODS

There are many approaches, each with many parameters, for producing adjustable lightweight grazing-incidence mirror modules. In this section we outline the rationale and briefly describe the methods we plan to use to address key questions.

2.1 Analytical and Finite Difference Modeling

The de facto standard for structural analysis is finite element method (FEM). Because of the relative simplicity of the objects of interest, thin shell segments, we have chosen to begin with a more analytical approach of simply numerically solving 2-dimensional differential equations with appropriate boundary conditions. The rationale is that these algorithms can be quickly implemented and modified in a high level language such as *Mathematica*® and are significantly quicker to execute. In addition, this approach requires no additional expense and training, and much less early involvement by our fully subscribed trained FEM experts.

We are in the process of implementing a finite difference deflection model based on Kirchhoff's plate bending theory (1850), and Donnell-Mushtari-Vlasov (DMV) shallow shell theory.[30] We numerically solve equations involving the *biharmonic* operator with boundary conditions. The biharmonic is a twice-applied Laplacian. We approximate the influence of piezoelectric actuators with a force distribution. For curved plates we are implementing the numerical solution to a pair of 4th order equations with boundary conditions, however due to time constraints, we have not yet reached the point of obtaining results. For now, we are using influence functions from FEM for curved shell segments.

Table 2. Summary of Kirchhoff plate and DMV shallow shell theories.

Kirchhoff	DMV
$\nabla^4\eta(x,y) = p(x,y)/D$, $\eta(x,y)$ = deflection in plate coordinates, $p(x,y)$ = pressure distribution orthogonal to the plate, and D = flexural rigidity = $\frac{Eh^3}{12(1-\nu^2)}$, where E = is Elastic Modulus, h = thickness, and ν = Poisson's Ratio.	$\nabla^4\eta(x,y) = (p(x,y) + \frac{1}{R\cos^2\frac{\Theta}{4}}\frac{\partial^2\Phi(x,y)}{\partial y^2})/D$, $\nabla^4\Phi(x,y) = -Eh\frac{1}{R\cos^2\frac{\Theta}{4}}\frac{\partial^2\eta(x,y)}{\partial y^2}$, $\Phi(x,y)$ = Airy stress function, Θ = shell azimuthal extent, and R = shell radius.

Validation

We compared the finite difference (FD) solutions to FEM solutions with modeled piezoelectric actuators. We modeled a 16 cm x 10 cm simply constrained flat, with 5 mm x 5 mm square piezoelectric pads separated by 0.5 mm. Glass thickness was 0.4 mm and piezoelectric material thickness was 0.2 mm. The FEM mesh was automatically generated using Comsol®. The finite difference model was gridded on 0.25 mm spacing (257041 elements). The finite difference model approximates piezoelectric actuation with a distribution of localized forces as shown in fig. 2. Results are compared in fig. 3, indicating very good agreement.

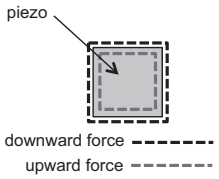

Figure 2. 2-D influence functions are approximated in FD by upward and downward force distributions.

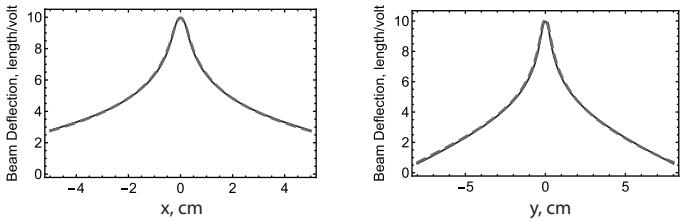

Figure 3. 2-D influence functions for FD (solid) and FEM (dashed) cases indicate that approximating the piezoelectric layers as force distributions is adequate for our needs.

2.2 Surface error map generation

Initially, we are using Monte Carlo technique to generate figure error maps. Because bimorph response is limited in bandwidth to spatial wavelengths longer than twice the actuator spacing and we are simply assuming linear bimorph influence, we may find it more efficient later to simply operate on Fourier components instead. We begin to quantify effects using these simulated error maps. We assume the following surface error spectrum.

$$f(\sigma_s,\omega) = \sigma_s\sqrt{\frac{\sin\frac{3\pi}{k}}{\pi(k-3)\lambda}}\,\frac{k\lambda^{k-1}}{\lambda^k+\omega^k},$$

where σ_s is the RMS slope error,
ω is the spatial frequency,
k is the assymptotic power law index and,
λ is a cutoff parameter to tune the low frequencies.

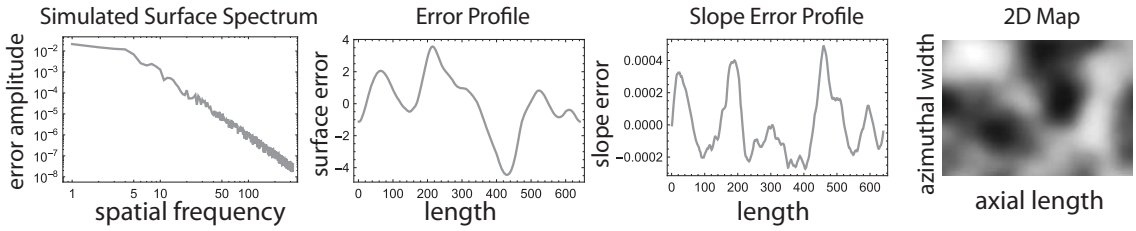

Figure 4: Examples of simulated surface error maps

The surface map is the discrete inverse Fourier transform of this spectrum. We randomly generated phases over $\pm\pi$ and 0.5-2.0× amplitude factors to produce a series of similar surface maps. The spectrum allows is the freedom to adjust *l* to match the Nyquist frequency set by the actuator spacing and adjust *k* to control high frequency content. These combine to set the performance floor. For 2-dimensional maps we let:

$$\omega \to |\omega_x + i\omega_y|,\ \lambda \to \lambda\sqrt{\frac{2a^2}{a^2+1-(a^2-1)\cos 2\arg(\omega_x+i\omega_y)}}$$

for axial and azimuth frequencies, $\{\omega_x, \omega_y\}$. The parameter a enables adjustment of the azimuthal spatial PSD relative to the axial one, since typically the azimuthal figure errors of actual segments will begin to decrease at lower spatial frequencies than axial ones. One and two-dimensional examples are shown in fig. 4.

2.3 1D Illustration

To introduce the approach, we apply simple beam theory to illuminate questions in 1 dimension. Fig. 5 compares influence functions for a Fixed mount vs. the simply supported case. This illustrates immediately that influence functions are different for a beam with fixed ends, vs. an unconstrained beam and that actuator effectiveness depends on position relative to the mounting locations. We observe that actuators are relatively ineffective near mounting points. Therefore, the completeness of resulting basis composed of the full set of influence functions is affected by mounting, and thereby the resulting performance improvement is also affected.

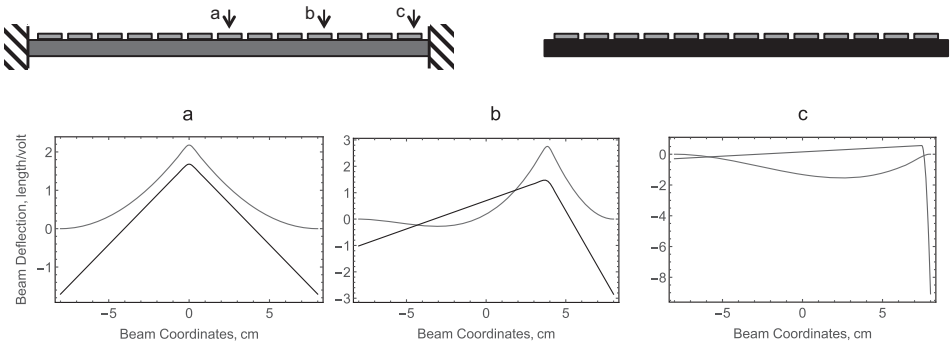

Figure 5: Comparison of fixed and unconstrained influence functions for a beam.

Figure 6(left) details a simple one-dimensional comparison between unconstrained and fixed mounting configurations. A beam with 4.4 arcsec initial RMS slope errors improves to 0.48 in the unconstrained case while improving only to 0.71 in a fixed configuration. The far right panel in figure 6 shows a statistical sampling and indicates that the slope errors at the ends tend to drive the performance in the fixed mounting case. This suggests that better results will be obtained for cases where either the correcting control efforts are enabled during the mounting process or where a flexure design is implemented which minimizes the ability of the interface to apply a bending moment at the mounting points.

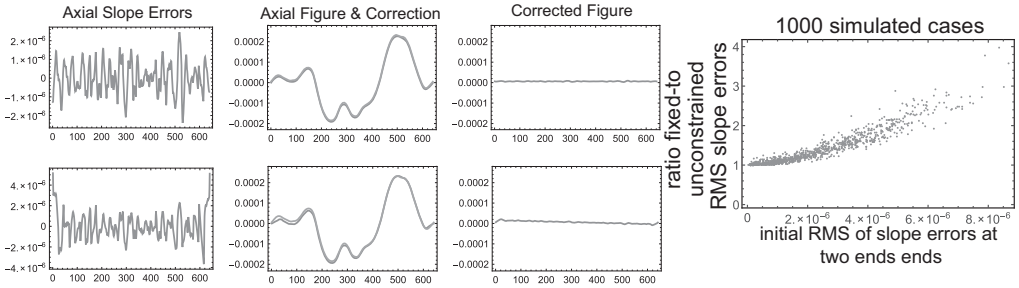

Figure 6: Unconstrained (upper) vs. fixed (lower). A mounting configuration, which fixes the initial slope errors at the mounting points, can result in substantially higher RMS slope errors, in this case the result is

3. INITIAL RESULTS

This section describes our initial findings for a simple plate and curved shell segments. At this early stage of investigation, our findings are blatantly obvious, but as we proceed we expect some more obscure subtleties to emerge.

3.1 Configuration

Our initial configuration is the minimal concept, described in sec 2.1.1. We consider a flat, a 30 cm radius shell segment, and a 15 cm radius shell segment. The FD model is used for the flat and FEM is used for the shell segments. The environment is zero-g and isothermal.

3.2 2-D Flat

A flat is a somewhat simpler implementation of the finite difference approach so we performed the preliminary validation described in sec. 2.1.1 in this configuration. Influence functions on the 2-D grid are fit to the error maps. We began by investigating the relative merit of assigning control efforts to minimize the surface deviation from prescription as opposed to minimizing the axial slope errors. The azimuthal figure is less important than the axial figure in x-ray optics because the two-reflection ray errors induced by azimuthal slope errors arise from $\Delta r/f$, and $r/f \times d\ln r/d\theta$ terms. These are likely to be negligible for long focal lengths, f, and typical azimuthal slope errors, $d\ln r/d\theta$. Figure 7 provides an illustration of a ~10 arcsec surface, which improves to 3 arcsec when fitted to minimize axial slope errors, while being limited to 3.5 arcsec for the other case. It is not surprising that better performance results from minimizing axial slope errors. But which results in better performance after mounting? The residual deviations from the prescribed surface may be substantial, and need to be budgeted in the alignment and mounting processes.

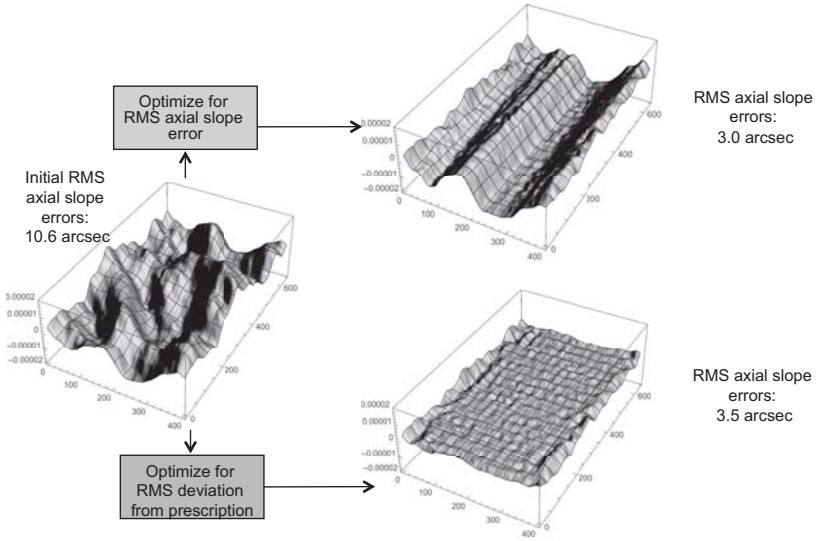

Figure 7: Dependence of the corrected surface on choice of control effort optimization parameter. Fitting to minimize axial slope errors gives a significantly better RMS axial slope error surface, but depending on the initial azimuthal figure it may impact mounting tolerances, or final two-reflection performance.

We also note that the results depend significantly on how we simulate the error map. The performance floor depends on the uncorrectable high spatial frequency component. We allow *k* from surface model in sec 2.2 to vary over the range 3-4 for this reason.

3.3 Dependence on shell segment radius

Influence functions on curved optics can differ significantly from flat due to the effective rigidity caused by the curvature in the azimuthal direction. Differences in influence functions are shown in fig. 8 for ∞, 30 cm, and 15 cm radii. The central displacement per unit excitation voltage for these influence functions is smaller for smaller radii, while that at the edge stays about the same. The surface deforms more along the azimuthal direction than the axial direction, so edge displacement for a given central displacement is larger. In fact, optimizing for axial slope errors alone actually

degrades the azimuthal figure by an increasing fraction with decreasing radii. This too must be included in the analysis of mounting distortions.

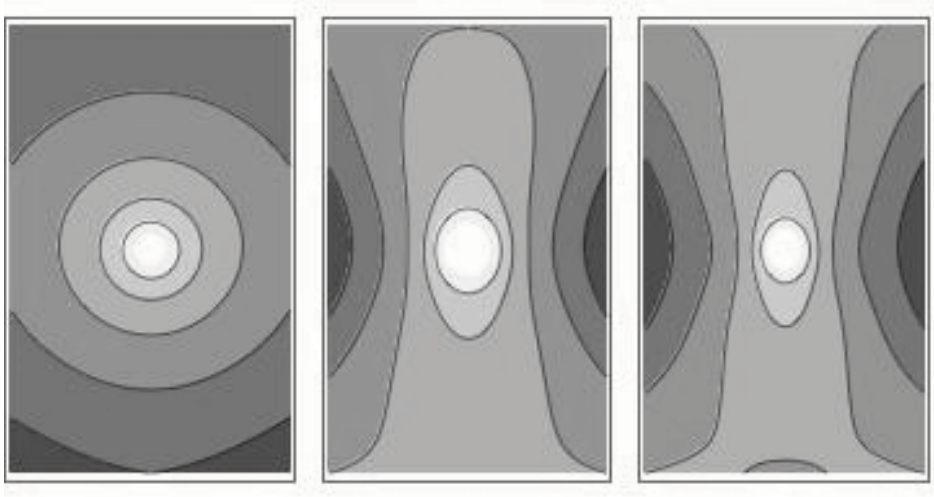

Figure 8: 2-D influence functions for a flat, a 30 cm radius shell segment, and a 15 cm radius shell segment. The flat case was determined by FD analysis while the two curved segments were modeled by FEM.

A simple performance comparison is shown in figure 9 for flat vs. 15 cm radius segments. For these we averaged the results from 1000 simulated surface error maps. We define *improvement factor* as the ratio of corrected to uncorrected RMS slope errors. The improvement factor is plotted against the asymptotic power law parameter, *k*, for a given set of simulated surface error maps. Increasing *k* produces less high spatial frequency power. Lower points are RMS axial slope error optimized and upper points are RMS prescription error minimized. We conclude that it is difficult to obtain good improvement factors in RMS axial slope error when optimizing RMS prescription error for smaller radius optics. In our future investigations it will be interesting to investigate how the azimuthal figure is affected by optimizing the axial slope errors of curved segments, and how this affects mounting strategies.

Optimizing segment spacing with respect to bimorph centers can further enhance performance. We noticed that fit residuals contain a consistent sinusoidal pattern correlated with the bimorph pattern. This arises from the fact that we assume a steep power law in the surface PSD, and that the highest correctable spatial frequency is the Nyquist frequency defined by the bimorph spacing. Because the influence functions are somewhat symmetric about the bimorph centers the correction is better in-phase than 90° out-of-phase at this frequency. This leads to residuals, which are dominated by the out-of-phase Nyquist frequency. Since this would be the case for all similar segments, it is possible to partially cancel these by optimizing primary-secondary spacing so that the residual slope error phases match.

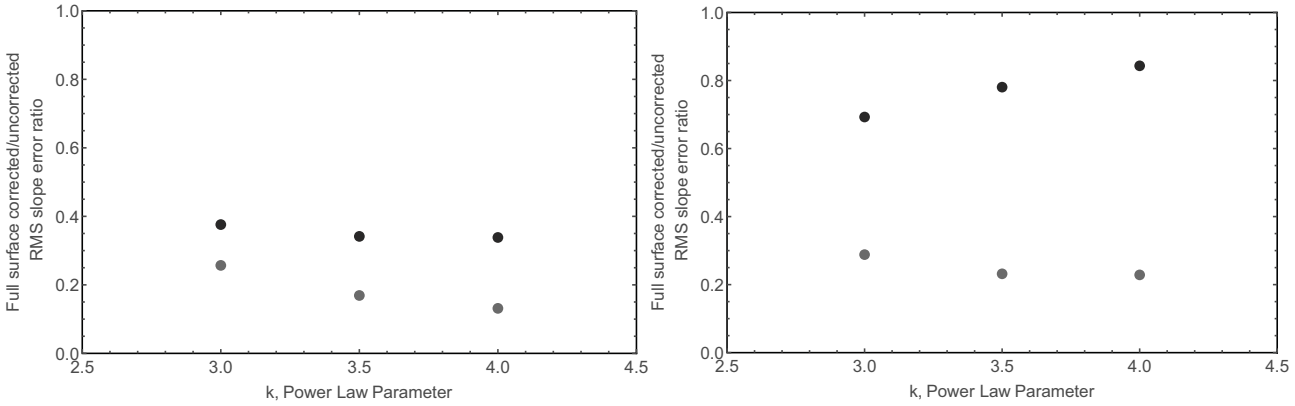

Figure 9: Flat vs. 15 cm radius segments, average of 1000 simulated surface error maps. Gray (lower) points are RMS axial slope error optimized; black (upper) points are RMS prescription error minimized.

Performance improvement by figure matching primary-secondary mirror pairs is also achievable. For independent error distributions, performance is $\sim 2\sqrt{2}\times$ RMS slope error. This would be reduced by a factor of $\sqrt{1-R}$ if errors were correlated, with correlation coefficient, R. Since metrology is required on each mirror to perform the corrections, the information to perform this matching would be available. A specific case worth of further investigation is where primary-secondary pair slope errors are matched only at mounting points, so as to minimize residual uncorrectable distortions.

The answer to the question of relative performance between a pair of adjustable segments, compared with 1-adjustable and 1-fixed segment, has the potential to affect the cost of the system. This model is linear, and not yet constrained to account for actuator limits and nonlinearities. In this case performance results are the same for separate correction of 2 mirrors and correction of either mirror by the axial slope error differences. However, there may be higher order and nonlinear effects. The discussion of spacing optimization for the out-of-phase Nyquist frequency still applies in this case. Additional mounting constraints arise from the need to match segment slope errors at mounting points. If the corrections in the adjustable optic are metrology driven rather than analysis driven, the metrology to correctly adjust this optic for mounting distortions in the fixed one may not be available, so the only option might be a nearly bending-moment-free flexure design.

3.4 Future Plans

We plan to expand the finite difference approach to curved segments (shallow shells) and full shells, develop an interface to efficiently investigate larger parameter spaces, develop and test prototypes of promising concepts. The next stage of analysis will be to add the required complexities: primary-secondary interface, effects of gravity load,[25] effect of gravity on the segments during metrology, detailed mount features.

We expect that the alignment precision needed for arcsec quality optics will require an integration of structural designs and assembly techniques into a system level process simulation rather than simply a statics model. As with the results above, we plan to begin with simple concepts, which provide adequate fidelity to identify tall poles and clear optimization paths. We will assess these concepts with a set of tools, which span the entire manufacturing and integration cycle while weighing factors that affect performance and performance per unit cost. We intend to continue to develop this analytical capability as an augmentation to our contributions in the area of testing as we begin to advance the technical readiness of active optics.

4. SUMMARY

Like any Wolter-I type optic, we need to manage the error budget for the difference in axial slope errors between the primary and secondary pairs. For this the terms include those due to figure errors and those due to alignment errors. Figure error contributions arise from uncorrected initial figure errors, and uncorrected induced distortions from gravity, thermal variations, temporary mounting for metrology and alignment fixtures, and bonds for alignment and integration into modules. Alignment error contributions include pair-to-pair variations in alignment arising from precision of alignment fixture, and precision of bonding process to alignment structures.

Although we've only investigated the key questions for mounting active optics for a short time, we have begun to draw some conclusions. Figure control impacts on mounting strategy appear to be minimal. It is better to have control activated during steps when segments are temporarily or permanently mounted. It will be necessary to remove mounting distortions from metrology data so they are not added to the final figure error. The accuracy that distortions are known determines how well they can be corrected so precise validation of model fidelity against test data is warranted. Optimizing figure control to minimize axial slope errors does not lead to improved azimuthal figure. Selection of matched pairs based on axial figure correlation could further improve performance. Adjustment capability on only one mirror appears to provide similar performance improvement to having it on both. Finally, if controlling figure on both primary and secondary, space segments to cancel lowest uncorrected frequency in the periodic correction residuals. This is a rather obvious laundry list of somewhat minor points, however we expect that as we complete this initial effort, we will continue to gain valuable insights. The small amount of effort we have expended thus far has increased our understanding and optimism at regarding the potential of adjustable optics technology.

REFERENCES

[1] Weisskopf, M. C., Aldcroft, T., Bautz, M., Cameron, R., Dewey, D., Drake, J., Grant, C., Marshall, H., & Murray, S.S., "An Overview of the Performance of the *Chandra X-ray Observatory*," Exp. Astron., 16, 1–68, (2003).

[2] Weisskopf, M. C., Brinkman, B., Canizares, C., Garmire, G., Murray, S., & Van Speybroeck, L., "An Overview of the Performance and Scientific Results from the *Chandra X-Ray Observatory*," Pub. Astron. Soc. Pac., 114, 1–24, (2002).

[3] Weisskopf, M. C., Tananbaum, H., Van Speybroeck, L., & O'Dell, S., "*Chandra X-ray Observatory* (CXO): overview," SPIE 4012, 2–16, (2000).

[4] Schwartz, D. A., "Invited Review Article: The Chandra X-ray Observatory," RScI 85, 061101- (2014).

[5] O'Dell, S. L., Aldcroft, T. L., Atkins, C., Button, T. W., Cotroneo, V., Davis, W. N., Doel, P., Feldman, C. H., Freeman, M. D., Gubarev, M. V., Johnson-Wilke, R. L., Kolodziejczak, J. J., Lillie, C. F., Michette, A. G., Ramsey, B. D., Reid, P. B., Rodriguez Sanmartin, D., Saha, T. T., Schwartz, D. A., Trolier-McKinstry, S. E., Ulmer, M. P., Wilke, R. H. T., Willingale, R., & Zhang, W. W., "Toward active x-ray telescopes II," SPIE 8503, (2012).

[6] Bavdaz, M., Wille, E., Wallace, K., Shortt, B., Fransen, S., Rando, N., Collon, M., Ackermann, M., Vacanti, G., Gunther, R., Haneveld, J., Olde Riekerink, M., Koelewijn, A., van Baren, C., Kampf, D., Zuknik, K.-H., Reutlinger, A., Christensen, F., Della Monica Ferreira, D., Jakobsen, A. C., Krumrey, M., Müller, P., Burwitz, V., Pareschi, G., Ghigo, M., Civitani, M., Proserpio, L., Spiga, D., Basso, S., Salmaso, B., Gallieni, D., Tintori, M., Fumi, P., Martelli, F., Parodi, G., Ferrario, I., & Povey, I., "X-ray optics developments at ESA," SPIE 8861, (2013).

[7] Zhang, W. W., Biskach, M. P., Blake, P. N., Chan, K.-W., Gaskin, J. A., Hong, M. L., Jones, W. D., Kolos, L. D., Mazzarella, J. R., McClelland, R. S., O'Dell, S. L., Saha, T. T., & Sharpe, M. V., "Next generation astronomical x-ray optics: high angular resolution, light weight, and low production cost," SPIE 8443, (2012).

[8] Zhang, W. W., Biskach, M. P., Blake, P. N., Bly, V. T., Carter, J. M., Chan, K. W., Gaskin, J. A., Hong, M., Hohl, B. R., Jones, W. D., Kolodziejczak, J. J., Kolos, L. D., Mazzarella, J. R., McClelland, R. S., McKeon, K. P., Miller, T. M., O'Dell, S. L., Riveros, R. E., Saha, T. T., Schofield, M. J., Sharpe, M. V., & Smith, H. C., "High resolution and high throughput x-ray optics for future astronomical missions," SPIE 8861, (2013).

[9] Cash, W., McEntaffer, R., Zhang, W., Casement, S., Lillie, C., Schattenburg, M., Bautz, M., Holland, A., Tsunemi, H., & O'Dell, S., "X-ray optics for WHIMex: the Warm Hot Intergalactic Medium Explorer," SPIE 8147, (2011).

[10] Kilaru, K., Ramsey, B. D., Gubarev, M. V., Gaskin, J. A., O'dell, S. L., & Zhang, W., "Differential deposition to correct surface figure deviations in astronomical grazing-incidence x-ray optics," SPIE 8147, (2011).

[11] Reid, P. B., Aldcroft, T. L., Cotroneo, V., Davis, W., Johnson-Wilke, R. L., McMuldroch, S., Ramsey, B. D., Schwartz, D. A., Trolier-McKinstry, S., Vikhlinin, A., & Wilke, R. H. T., "Technology development of adjustable grazing incidence x-ray optics for sub-arc second imaging," SPIE 8443, (2012).

[12] Citterio, O., Civitani, M. M., Pareschi, G., Basso, S., Campana, S., Conconi, P., Ghigo, M., Mattaini, E., Moretti, A., Parodi, G., & Tagliaferri, G., "Thin fused silica optics for a few arcsec angular resolution and large collecting area x-ray telescope," SPIE 8861, (2013).

[13] Civitani, M. M., Campana, S., Citterio, O., Conconi, P., Pareschi, G., Tagliaferri, G., & Parodi, G., "High angular resolution optics for the next generation of wide field X-ray telescopes beyond e-Rosita," MmSAI 84, 817-(2013).

[14] Murray, S. S., Borgani, S., Campana, S., Citterio, O., Forman, W., Giacconi, R., Gilli, R., Paolillo, M., Pareschi, G., Ptak, A., Rosati, P., Tozzi, P., Weisskopf, M., & the WFXT Team, "Wide Field X-ray Telescope (WFXT)," MmSAI 84, 790-(2013).

[15] Ulmer, M. P., Wang, X., Cao, J., Graham, M. E., & Vaynman, S., "Update to an application using magnetic smart materials to modify the shape of an x-ray telescope mirror," SPIE 8861, (2013).

[16] Atkins, C., Ramsey, B., Kilaru, K., Gubarev, M., O'Dell, S., Elsner, R., Swartz, D., Gaskin, J., & Weisskopf, M., "X-ray optic developments at NASA's MSFC," SPIE 8777, (2013).

[17] Ramsey, B. D., Engelhaupt, D., Speegle, C., Austin, R., Kolodziejczak, J., O'Dell, S. & Weisskopf, M., "The HERO Program, High-Energy Replicated Optics for a Hard-X-Ray Balloon Payload," SPIE 3765, 816-821 (1999).

[18] Gubarev, M., O'Dell, S., Elsner, R., Kilaru, K., Atkins, C., Swartz, D., Gaskin, J., & Weisskopf, M., "Flight programs and X-ray optics development at MSFC," MmSAI 84, 821- (2013).

[19] Gubarev, M., Ramsey, B., O'Dell, S. L., Elsner, R., Kilaru, K., McCracken, J., Pavlinsky, M., Tkachenko, A., Lapshov, I., Atkins, C., & Zavlin, V., "Development of mirror modules for the ART-XC instrument aboard the Spectrum-Roentgen-Gamma mission," SPIE 8861, (2013).
[20] Krucker, S., Christe, S., Glesener, L., Ishikawa, S.-n., McBride, S., Glaser, D., Turin, P., Lin, R. P., Gubarev, M., Ramsey, B., Saito, S., Tanaka, Y., Takahashi, T., Watanabe, S., Tanaka, T., Tajima, H., & Masuda, S., "The Focusing Optics X-ray Solar Imager (FOXSI)," SPIE 8147, (2011).
[21] Ramsey, B. D., Atkins, C., Gubarev, M. V., Kilaru, K., & O'Dell, S. L., "Optics requirements for x-ray astronomy and developments at the Marshall Space Flight Center," NIMPA 710, 143-150 (2013).
[22] Roche, J. M., Kolodziejczak, J. J., O'Dell, S. L., Elsner, R. F., Weisskopf, M. C., Ramsey, B., & Gubarev, M. V., "Opto-mechanical analyses for performance optimization of lightweight grazing-incidence mirrors," SPIE 8861, (2013).
[23] Schwartz, D. A., Allured, R., Bookbinder, J., Cotroneo, V., Forman, W. R., Freeman, M. D., McMuldroch S., Reid, P. B., Tananbaum, H. D., Vikhlinin, A. A., Johnson-Wilke, R. L., Trolier-McKinstry, S. E., Wilke, R. H. T., Gubarev, M., Kolodziejczak, J., O'Dell, S. L., Ramsey, B. D., "Technology requirements for a Square-Meter Arcsecond-Resolution Telescope for X-rays: the SMART-X mission," SPIE 9208, (2014).
[24] Cohen, L. M., Cernoch, L. J., Matthews, G., & Stallcup, M. A., "Structural considerations for fabrication and mounting of the AXAF HRMA optics," SPIE 1303, 162-177 (1990).
[25] Schwartz, D. A., Cotroneo, V., Davis, W., Freeman, M., & Reid, P., "Adjustable x-ray optics: correction for gravity-induced figure errors," SPIE 8147, (2011).
[26] Doyle, K., Genberg, V., & Michels, G., [Integrated Optomechanical Analysis], SPIE Press, Bellingham WA, (2012).
[27] Arenberg, J., Matthews, G., Atkinson, C., Cohen, L., Golisano, C., Havey, Jr., K., Hefner, K., Jones, C., Kegley, J., Knollenberg, P., Lavoie, T., Oliver, J., Plucinsky, P., Tananbaum, H., Texter, S., Weisskopf, M., "Lessons we learned designing and building the Chandra telescope," SPIE 9144, (2014).
[28] Weisskopf, M., "Fifteen years of Chandra operation: scientific highlights and lessons learned," SPIE 9144, (2014).
[29] Schwartz, D., "Lessons from the development and operation of the Chandra x-ray observatory," SPIE 9144, (2014).
[30] Ventsel, E., & Krauthammer, T., [Thin Plates and Shells, Theory, Analysis, and Applications], Marcel Dekker Inc., New York, (2001).